NREL/CP-520-22949 • UC Category: 1250

Comparison of Close-Spaced Sublimated and Chemical Bath Deposited CdS Films: Effects on CdTe Solar Cells

D. Albin, D. Rose, R. Dhere,
D. Levi, L. Woods, A. Swartzlander,
and P. Sheldon

Presented at the 26th IEEE Photovoltaic Specialists Conference, September 29–October 3, 1997, Anaheim, California

National Renewable Energy Laboratory
1617 Cole Boulevard
Golden, Colorado 80401-3393
A national laboratory of the U.S. Department of Energy
Managed by Midwest Research Institute
for the U.S. Department of Energy
under contract No. DE-AC36-83CH10093

Prepared under Task No. PV704201

September 1997

COMPARISON STUDY OF CLOSE-SPACED SUBLIMATED AND CHEMICAL BATH DEPOSITED CdS FILMS: EFFECTS ON CdTe SOLAR CELLS

D. Albin, D. Rose, R. Dhere, D. Levi, L. Woods, A. Swartzlander, and P. Sheldon
National Renewable Energy Laboratory, CO 80401

ABSTRACT

Close-spaced-sublimated (CSS) CdS films exhibit strong fundamental edge luminescence, high optical absorption, and a bandgap of ~2.41 eV. Structurally, these films show good crystallinity with thickness-dependent grain sizes that vary between 100-400 nm. In contrast, chemical-bath-deposited (CBD) CdS exhibits subband luminescence, lower absorption, and a thickness-dependent bandgap. These films have CdS grains typically less than 50 nm in size and poorer crystallinity. However, CdTe devices fabricated with these lower "quality" CBD CdS films yield higher V_{oc}'s and fill factors. Carrier lifetimes in finished CSS CdS devices measured between 100 and 200 ps while lifetimes in CBD CdS devices were much higher (>500 ps). Compositional differences in the Cd/(S+Te) ratio at the interface suggest the possibility of lower CdS doping and higher CdTe compensation as one reason for lower V_{oc}'s in CSS CdS devices.

INTRODUCTION

CdTe superstrate solar cells require the use of a thin n-type CdS window layer between the n-type transparent conductor oxide (TCO) and the p-type CdTe absorber. The current process for fabricating the highest-efficiency CdTe solar cells uses close-spaced-sublimation and chemical-bath-deposition for growing the CdTe and CdS layers respectively [1]. The latter CBD process is questionable as a manufacturing process which has promoted recent interest in both CSS and chemical-vapor-deposited (CVD) CdS [2,3]. Both processes require the use of higher substrate temperatures than what is encountered in films grown by solution chemistry (typ.~100°C). Until recently, CdTe devices made from CSS-grown CdS yielded lower V_{oc}'s and consequently lower efficiencies than devices made with CBD-grown CdS films [4]. The latter improvements were based upon incorporating oxygen during the CdS growth leading to significant CdO formation. In this paper, we first characterize differences in the morphology and optical properties of as-grown CBD and CSS CdS films grown entirely in He ambients. Next, we then fabricate CdS/CdTe devices using these films and identify differences that exist at CSS CdS/CdTe and CBD CdS/CdTe interfaces. By this approach, the groundwork for improving the performance of CSS CdS/CdTe devices is established.

EXPERIMENTAL APPROACH

Corning 7059 glass was used as the substrate in all film depositions. TCO's consisted of SnO_2 grown by either tetramethyl-tin or stannous chloride CVD. CBD CdS films were grown by a "standard" process consisting of a solution containing 550 ml H_2O, 8 ml of 0.033 M Cd-acetate solution, 4.7 ml of 1.0 M ammonium acetate solution, and 15 ml of 14.76 M NH_4OH solution titrated with 8 ml of 0.067 M thiourea solution. CSS CdS films were grown by sublimating pulverized 99.999% CdS powder in 10 torr of helium onto SnO_2/glass substrates heated to ~475 °C. In both cases, CdS film thickness was controlled by varying deposition time. CBD film depositions typically required 35-40 minutes deposition time while CSS film depositions required 4-15 minutes. With exception of the type of CdS used, film thickness was the primary CdS variable used in this study.

To provide a true comparison of the effects of CSS and CBD CdS films, the CdTe film deposition and post deposition device processing were kept fairly constant and have been described in detail previously [5]. CdTe depositions typically were performed by pre-annealing the CdS/SnO_2/Glass substrates in H_2 at 300°C followed by the CdTe deposition in an ambient of 1 torr O_2 and 15 torr helium. CdTe thickness for devices was approximately 10 μm.

A large number of CdTe depositions were also performed in which the CdTe film thickness was controlled to ~1000-3000 Å, with substrate temperatures of 525 and 600°C, and oxygen partial pressures of 0, 1, and 2 torr. These "thin-film couples" were used as samples for optical and grazing-incidence X-ray diffraction (GIXRD) characterization of the CdS/CdTe interface. A "lift-off" procedure was also developed for separating CdS/thick CdTe interfaces near the metallurgical junction. Subsequent analysis could then be performed on the exposed alloy surface directly. These latter thick-film "lift-off samples" consisted of 10-μm-thick CdTe films and consequently, should be more representative of actual device interfaces.

Optical measurements consisted of both time-resolved photoluminescence (TRPL) to measure carrier lifetimes in CdTe both before and after wet-$CdCl_2$ treatment of the CdS/CdTe layers, and specular (non-integrating) R,T

measurements of thin-film couples. I-V device measurements were performed using a xenon-arc lamp simulator calibrated with NREL-confirmed devices. I-V curves were also used to extract the series-resistance-corrected, reverse saturation dark current, J_o. External quantum efficiency (QE) measurements were performed using zero-light bias with total integrated current set to the measured J_{sc} of each device.

Finally, morphology and compositional data were obtained with scanning electron microscopy (SEM), atomic-force microscopy (AFM), and Auger electron spectroscopy (AES).

RESULTS AND DISCUSSION

The higher substrate temperatures available to CSS-grown CdS films relative to CBD CdS films resulted in marked differences in grain size, crystallinity, and optical properties. As shown in Fig. 1, CdS grown by CSS is much larger-grained than CdS grown by CBD . Although substrate temperature cannot significantly change CBD CdS grain size [6], CSS grain size can be varied by controlling both substrate temperature and film thickness. In this study, grain size was observed to vary from ~100 nm for very thin (575 Å) CSS CdS films up to nearly 300-400 nm for thicker (3060 Å) films. CBD CdS grain sizes were limited to around 30-50 nm for films thinner than 1500 Å. Thinner CBD CdS films result in a slight decrease in grain size. CSS-grown CdS films were shown to have better crystallinity (as shown by higher XRD intensities) than CBD-grown CdS. CSS films consisted primarily of hexagonal phase CdS with CBD CdS films containing primarily the cubic form.

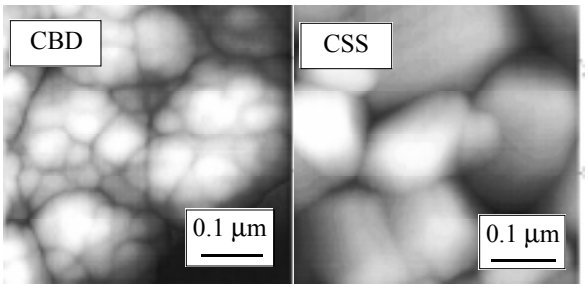

Fig. 1. AFM images of CBD and CSS grown CdS films

Optically, CSS films were found to differ significantly from CBD grown CdS films. Room-temperature PL using pulsed 400 nm excitation light showed a strong PL peak for CSS CdS at 2.43 eV with only slight subband luminescence. In contrast, luminescence in CBD-grown CdS was dominated by a broad, subband peak centered at 1.78 eV. Absorption coefficients, calculated from R,T measurements, also showed less bandtails and somewhat higher absorption coefficients for CSS-grown CdS. The bandgap of CBD-grown CdS films was also found to vary significantly with film thickness which was not the case for CSS-grown CdS as shown in Fig. 2. Variations in bandgap with thickness for the CBD case are a result of the changing growth chemistry present during long CBD depositions. In contrast, the film growth mechanisms present during the CSS process are more invariant.

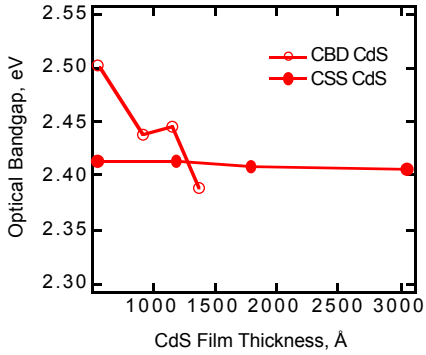

Fig. 2. CdS Bandgap vs. CdS film thickness

In polycrystalline solar cells, descriptives like large-grained structures, sharp bandedges, and direct-gap luminescence usually imply high quality. Unfortunately, higher quality films did not translate into higher quality devices. CSS-grown CdS films always yielded inferior devices relative to their CBD-grown counterparts.

V_{oc} as a function of the type of CdS (CBD or CSS), CdS film thickness, and the use (or absence) of wet $CdCl_2$ treatments is shown in Fig. 3. Significant differences in fill factor and efficiency for CBD and CSS-grown CdS devices were also observed. J_{sc} did not appear to be seriously affected by the type of CdS used.

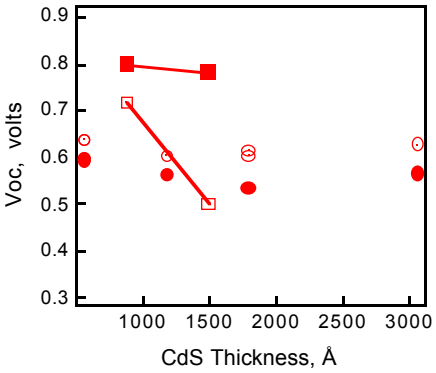

Fig. 3. I-V results comparing CSS (circles) and CBD (squares) CdS device V_{oc} both with (solid) and without (open) $CdCl_2$ as a function of CdS film thickness.

An interesting observation from Fig. 3 is that with CSS-grown CdS devices, $CdCl_2$ treatments appear to be detrimental to V_{oc}. This contradicts previous results with CBD-grown CdS in which such treatments raise V_{oc}. TRPL decay measurements showed that the decrease in V_{oc} with $CdCl_2$ could not be attributed to carrier lifetime. Rather,

lifetimes always improved with $CdCl_2$ treatment regardless of CdS type. CBD CdS devices exhibited carrier lifetimes of <200 ps before $CdCl_2$ and >500 ps after $CdCl_2$. CSS CdS devices had much smaller carrier lifetimes of 50-60 ps before $CdCl_2$ and 100-200 ps after $CdCl_2$. Reverse dark currents, J_o, were also larger in devices using CSS-grown CdS. The anomaly of both improved carrier lifetimes and smaller V_{oc} with $CdCl_2$ treatment of CSS CdS devices indicates that recombination may not be the only mechanism affecting the V_{oc} of these cells.

Relative shifts in QE long wavelength response to longer wavelengths (smaller bandgaps) both before and after $CdCl_2$ were used to determine the degree of $CdTe_{1-x}S_x$ alloying in the devices above. For both CSS and CBD CdS films, CdS-CdTe interdiffusion in non-$CdCl_2$ treated devices increased when thinner CdS films were used. Thinner CdS typically results in smaller grained morphologies, which can either affect S diffusion directly (through increased CdS surface area) or through affecting CdTe grain size (smaller CdTe grain nucleation). Alloying appeared to be slightly less in the CSS-grown CdS case, possibly because of grain size differences.

Differences in alloying between CSS and CBD-grown CdS films were best studied by GIXRD and AES. The use of lift-off samples where separation occurred near the original CdS/CdTe interface allowed direct analysis of the alloyed region, without the interfering effects of overlying CdTe. GIXRD scans (before $CdCl_2$) performed at incident angles above and below a theoretically-calculated total-reflection critical angle of 0.33° to monitor alloy formation are shown in Figure 4. In both sets (a) and (b), scans of increasing intensity correspond to increasing incidence angles of 0.2, 0.4, 0.9, 1.9, and 4.9 degrees. Also shown in (c) is the peak profile fit (split Pearson) of the alloy phase plotted as a function of the beam normal penetration depth into the CdTe alloy. Due to the convolution of smaller incident angle data, the actual penetration of the alloy phase can be expected to be somewhat less than that suggested in Fig. 4(c). Regardless, alloying is observed to be greater in terms of S-content and amount when CBD CdS films are used in pre-$CdCl_2$ devices. Such alloying is believed to improve V_{oc} by reducing interface states associated with lattice mismatching between CdS and CdTe [7].

GIXRD analysis of lift-off samples obtained after $CdCl_2$ showed increased peak broadening (possibly associated with recrystallization-strain effects) which made data interpretation difficult. Preliminary results reveal little difference in GIXRD-obtained alloy peak positions for the two types of CdS cases after $CdCl_2$ processing. The possibility that S-profiles after $CdCl_2$ are similar was also supported by AES depth profiling data, shown in Fig. 5, of lift-off samples, in which separation occurred near the original TCO/CdS interface in $CdCl_2$ treated films. As seen in this figure, there appears to be little difference in the distribution of S after $CdCl_2$ processing of CBD and CSS CdS/CdTe interfaces. There are however, subtle, but significant differences in various compositional ratios between the two.

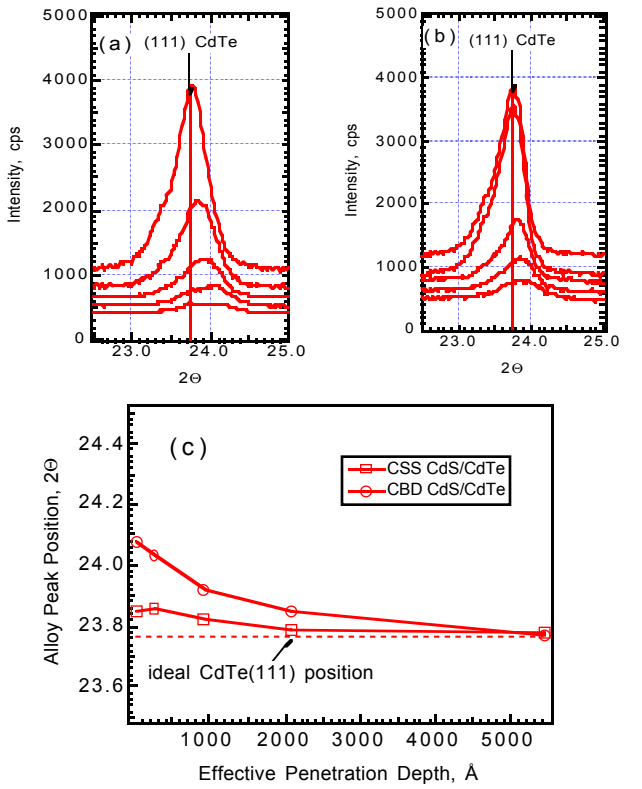

Fig. 4. GIXRD data of CdS/CdTe alloy region for (a) CBD-grown CdS and (b) CSS-grown CdS. Films were not treated with $CdCl_2$. Peak position corresponding to the (111) alloy peak position for both cases as a function of X-ray penetration depth is shown in (c).

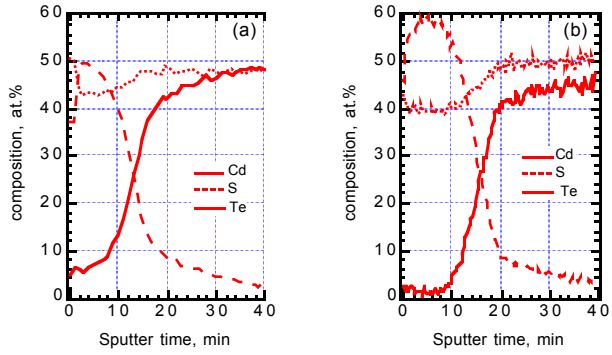

Fig. 5. AES depth profiles for Cd,S, and Te at the CdS/alloy/CdTe interface for CBD (a) and CSS (b) CdS films

From the data shown in Fig. 5, it appears that the ratio of Cd to anion (S+Te) on both sides of the interface depends on the type of CdS used. On the CdS side of the interface, CBD CdS films appear to be anion-deficient

relative to CSS CdS. This makes the likelihood for Cl_S donor type defects in CBD CdS more probable. On the CdTe side of the interface, it appears that CSS CdS films result in the growth of slightly more compensated Cd-rich alloy. Lower CdS doping and higher CdTe compensation can effectively reduce V_{oc} of CSS CdS devices by reducing the junction built-in voltage, V_{bi} [8]. The variation in cation to anion ratio across the CdS/CdTe interface is shown in Figure 6 below.

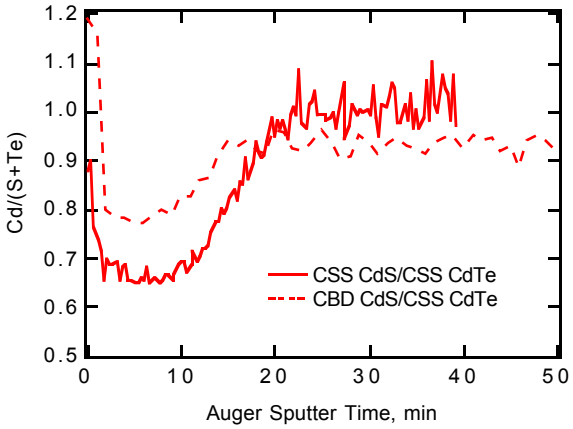

Fig. 6. Differences observed in cation to anion ratio between CSS and CBD CdS/CdTe interfaces

During the collection of AES data, it was observed that there was more sample charging of the CSS CdS sample resulting in a noiser signal as seen in Figs. 5 and 6. It is likely that this may be due to differences in the conductivity of the CdS layer. The large S-deficiency of CBD CdS and better likelihood of Cl_S doping or possibly, the larger amount of Te in these films may be responsible for the better conductivity of the CBD CdS layer. Sample charging can also result in AES measurement artifacts, in particular peak energy shifts and possibly intensity changes. In the data shown here, the magnitude of the charging was not felt to be significant enough to introduce these effects. This will be verified in future work.

Finally, optical absorption measurements of thin-film couples revealed an interesting difference between CdTe films grown on CSS and CBD-grown CdS films. As shown in Fig. 7, CdTe absorption appears to be enhanced nearly 50% when grown on CSS-CdS relative to growth on CBD-CdS. This increase in absorption may be due to an improvement in the density or crystallinity of the CdTe film near the interface, possibly associated with the larger-grained CSS CdS. Differences in either optical scattering or TCO type were eliminated as explanations for the absorption differences shown in Fig. 7. Calculations based upon single crystal CdTe absorption data show that nearly 90% of all incident AM 1.5 light transmitted through the TCO and CdS layers is absorbed within 6000 Å of the CdS/CdTe interface. Variations in absorption can significantly impact this optical generation function. An increase in absorption similar to that shown would move the 90% collection depth to within 3000 Å of the interface for the CSS CdS case.

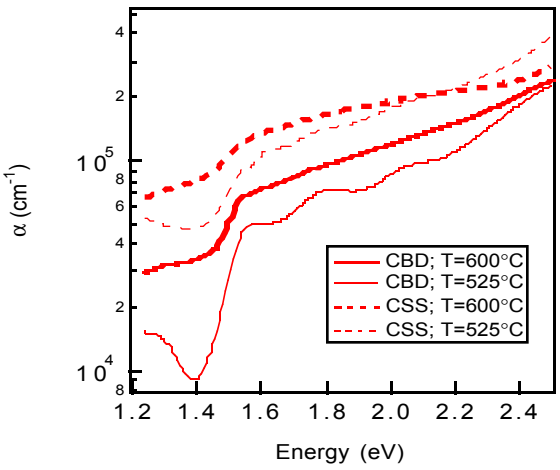

Fig. 7. Absorption coefficients of CdTe films grown on CBD and CSS CdS surfaces

SUMMARY

CSS-CdS films appear to be of much better quality than CBD-CdS films. Yet, the latter films yield much better devices. Significant differences in alloying, optical generation, and composition at the interface were identified. These differences may be responsible for the differences observed in device performance.

ACKNOWLEDGMENTS

This work was supported by the U.S. Department of Energy under contract No. DE-AC36-83CH10093 to NREL. We also wish to thank H. Moutinho and R. Matson for AFM and SEM measurements, and D. Dunlavey and K. Emergy for assistance in QE and I-V measurements.

REFERENCES

1. C. Ferekides, et al., *Proc. 23rd IEEE Photovoltaic Spec. Conf.,* (1993) p. 389.
2. C. Ferekides, et al., *Proc. 25th IEEE Photovoltaic Spec. Conf.,* (1996) p. 751.
3. T. Nishio, et al., *Proc. 25th IEEE PV Photovoltaic Spec. Conf.,* (1996) p. 953.
4. C. Ferekides, et al., ibid.
5. D. Albin, et al., *14th NREL/SNL Photovoltaics Program Review,* AIP Press, (1997) p. 665.
6. H.R. Moutinho, et al., *Proc. 25th IEEE Photovoltaic Spec. Conf.*, (1996) p. 945.
7. R. Dhere, et al., *13th NREL Photovoltaics Program Review, AIP Press*, (1995) p. 392.
8. J.R. Site, *Proc. 20th IEEE Photovoltaic Spec. Conf.*, (1988) p. 1604.